IOP Publishing Journal of Physics B: Atomic, Molecular and Optical Physics
J. Phys. B: At. Mol. Opt. Phys. **54** (2021) 245001 (12pp) https://doi.org/10.1088/1361-6455/ac44e1

# Spectroscopic analysis of M- and N-intrashell transitions in Co-like to Na-like Yb ions

**R Silwal[1,2,3,*], Dipti[1,6], E Takacs[1,2], J M Dreiling[1,7], S C Sanders[1,2], A C Gall[1,2,8], B H Rudramadevi[1,4], J D Gillaspy[1,5] and Yu Ralchenko[1]**

[1] National Institute of Standards and Technology, Gaithersburg, MD 20899, United States of America
[2] Department of Physics and Astronomy, Clemson University, Clemson, SC 29634, United States of America
[3] Department of Physics and Astronomy, Appalachian State University, Boone, NC, 28608, United States of America
[4] Department of Physics, SVU College of Sciences, Sri Venkateswara University, Tirupati, AP 517502, India
[5] National Science Foundation, Alexandria, VA 22314, United States of America

E-mail: silwalr@appstate.edu and yuri.ralchenko@nist.gov

Received 27 September 2021, revised 14 December 2021
Accepted for publication 19 December 2021
Published 11 February 2022

**Abstract**

The M-intrashell spectra from Co-like $Yb^{43+}$ through Na-like $Yb^{59+}$ ions produced in an electron beam ion trap (EBIT) at the National Institute of Standards and Technology have been studied in the extreme ultraviolet (EUV) range. A few N-intrashell transitions for Co-like $Yb^{43+}$ and Fe-like $Yb^{44+}$ are also reported. The EUV radiation was observed with a flat-field grazing incidence spectrometer in the wavelength region of about 7.5 nm to 26.2 nm. The electron beam energies were varied between 3.6 keV and 18 keV to produce the ionization stages of interest. The line identifications were based on the large-scale simulations of the EBIT plasma emission using the non-Maxwellian collisional-radiative code NOMAD. A total of 76 previously unobserved spectral lines corresponding to electric-dipole and magnetic-dipole transitions in the above mentioned ions were identified and discussed. In particular, our accurate wavelength of $24.3855 \pm 0.0005$ nm for a magnetic-dipole (M1) transition in the ground configuration of Co-like ion presents a solid benchmark for comparisons with the most advanced theories of atomic structure.

Keywords: EUV spectroscopy, ytterbium, electron beam ion trap, collisional-radiative modeling, magnetic-dipole lines

(Some figures may appear in colour only in the online journal)

## 1. Introduction

Atomic transitions of various charge states of Yb have been studied in the context of both fundamental and applied science. Measurement of transitions in ultracold Yb atoms and singly-ionized Yb ions allowed for the realization of highly accurate atomic clocks [1–5], including an optical lattice clock [1]. These atomic systems were studied extensively due to their potential application as trapped-ion frequency standards [2, 6, 7] and for quantum electrodynamics (QED) studies as well as quantum computation tests. Isotope shift measurements in singly charged $Yb^+$ ions were recently used for search for physics beyond the standard model [8]. Atomic data for the low charge states of Yb were also measured and calculated due to

* Author to whom any correspondence should be addressed.
[6] Present address: International Atomic Energy Agency, A-1400 Vienna, Austria.
[7] Present address: Honeywell Quantum Solutions, Broomfield, CO 80021, USA.
[8] Present address: Smithsonian Astrophysical Observatory, Cambridge, MA 02138, USA.

 © 2022 IOP Publishing Ltd Printed in the UK

their relevance in astrophysical plasmas and for the theoretical studies of their complicated configurations [6, 7].

In general, atomic transitions in the soft x-ray or low extreme-ultraviolet (EUV) regions of lanthanide elements ($Z_N = 57$–$71$) have been of interest due to their possible applications in EUV lithography (EUVL) [9–14] and in studies of relativistic and correlation effects [15, 16]. Of specific interest in EUVL are the N-shell 4p–4d and 4d–4f transitions that emit in the wavelength range near 13.5 nm. The shorter wavelength sources are considered suitable for EUVL plasmas since smaller feature sizes can be attained at these wavelengths [11].

Few atomic transitions in highly charged Yb ions have already been studied previously. For instance, the $n = 4$ to $n = 4$ transitions in Ni-like, Co-like, Zn-like, Cu-like, and Fe-like ions were produced and observed in tokamaks [17], laser-produced plasmas [17–20], the large helical device [15, 21], and electron beam ion traps (EBITs) [12–14, 22]. Recently, we reported a detailed study of the EUV measurements of the intrashell ($\Delta n = 0$, $n = 4$) in Rb-like $Yb^{33+}$ to Ni-like $Yb^{42+}$ ions produced at the EBIT facility at the National Institute of Standards and Technology (NIST) [23]. In this work, we extend the EUV measurements of few N-intrashell and M-intrashell transitions in Co-like $Yb^{43+}$ through Na-like $Yb^{59+}$ ions.

Previously, scarcely any measurements had been performed for the $n = 3$ to $n = 3$ transitions for lanthanides. For atomic structure calculations, accurate *ab initio* methods such as multi-configuration Dirac–Hartree–Fock (MCDHF), *R*-matrix, and relativistic many-body perturbation theory (RMBPT) have been developed for the one-electron Na-like [24, 25] and two-electron Mg-like Yb ions [26, 27]. Co-like ions, with the ground state configuration $3d^9$, provide a system with one hole in the 3d shell, equivalent to a one-electron system. Si *et al* [28] investigated the electron correlations, Breit, and QED corrections for the magnetic-dipole (M1) $3d^9\ ^2D_{3/2} \rightarrow {}^2D_{5/2}$ transition in Co-like ions along the isoelectronic sequence with the MCDHF method implemented in GRASP2K code [28, 29].

Except in the case of few-electron ions, the theory gets complicated and less accurate for many electron systems due to the increased electron–electron correlations. New measurements for the many-electron ions can therefore provide benchmark tests of the existing framework and are necessary for accurate tests of the QED theory in many-body systems. The magnetic-dipole transitions are important for diagnostics of laboratory and fusion plasmas [30, 31], and recent studies have suggested these transitions could be interesting for the development of ultra-precise optical atomic clocks [32]. We present the measurement of EUV emission from the NIST EBIT for the M-shell ions of Yb ($Yb^{43+}$–$Yb^{59+}$) that include electric-dipole and magnetic-dipole transitions.

## 2. Experimental approach

The EBIT facility at NIST was used to produce and trap the highly charged Yb ions. In the EBIT, an intense electron beam emitted by a high perveance electron gun is accelerated towards the trap region that consists of three drift tube electrodes. The acceleration is commensurate with the difference in applied electrical potentials between the cathode in the egun and the center drift tube in the trap. This potential difference defines, to first order, the electron beam energy, which must be corrected lower by the self-field or space charge of the electron beam. The electron beam is compressed to a radius of few tens of microns by a 2.7 T superconducting magnet surrounding the trap, and the width of the electron energy distribution function (approximately Gaussian) is about 40 eV. The element under investigation is injected to the trap region either as a neutral gas [33] or as singly charged ions from a metal vapor vacuum arc (MeVVA) ion source [34].

During this measurement, singly charged Yb ions were injected into the trap from the MeVVA source and captured by matching the MeVVA floating potential to the center drift tube potential [35]. The trapped Yb ions were further ionized by the highly focused electron beam through electron impact ionization. The axial trapping of the highly ionized Yb was accomplished by applying a higher voltage to the end drift tubes relative to the center drift tube to create a potential well. Radial trapping of the ions was realized by the space charge of the electron beam and the axial magnetic field of the superconducting magnet. At various intervals Ne atoms were injected into the trap as gas for the calibration of the EUV spectra. In addition, impurity ions: Xe, Ba, Ar, N, and O are usually present in the trap. Xe atoms are known to linger in the trap from previous measurements, Ba atoms come from the cathode of the electron gun, and Ar atoms from the EUV ion pumps.

The ionization energies for Co-like through Na-like charge states of Yb range from 3.5 keV to 6.2 keV, respectively. Therefore, electron beam energies of 3.6 keV and higher were used to produce the M-shell (Co-like through Na-like) charge states. The spectra at 3.6 keV and 3.75 keV were collected for 20 min each. For the higher electron beam energies, where higher charge states appear, the spectra were collected for longer times to improve the statistics. This is because the excitation cross sections decrease with higher electron beam energy. The electron beam current during the measurement varied between 135 mA and 145 mA. It has to be noted that the plasma reaches a steady state distribution in a fraction of a second, while the ions are trapped for a few seconds. The emitted radiation corresponds to a steady state plasma. The spectra for the Co-like through Na-like transitions are shown in figures 1 and 2. The intensity of the experimental spectra is given in analog-to-digital units (ADUs) and the theoretical data is normalized to the strongest line in the spectrum. The spectra at 18 keV was collected at a spectral window of 1.8–15.4 nm by moving the position of the detector. This was done to optimize the signal in the lower wavelength regions. The red curves in these figures correspond to the approximate the second order Yb spectra obtained by multiplying the wavelength of the first order experimental spectra by 2 and dividing the line intensities by 2.5, to visually aid the line identification [35].

The emission from the highly charged Yb plasma in the EUV region was recorded by a flat-field grazing incidence EUV spectrometer [36]. The light from the EBIT plasma is

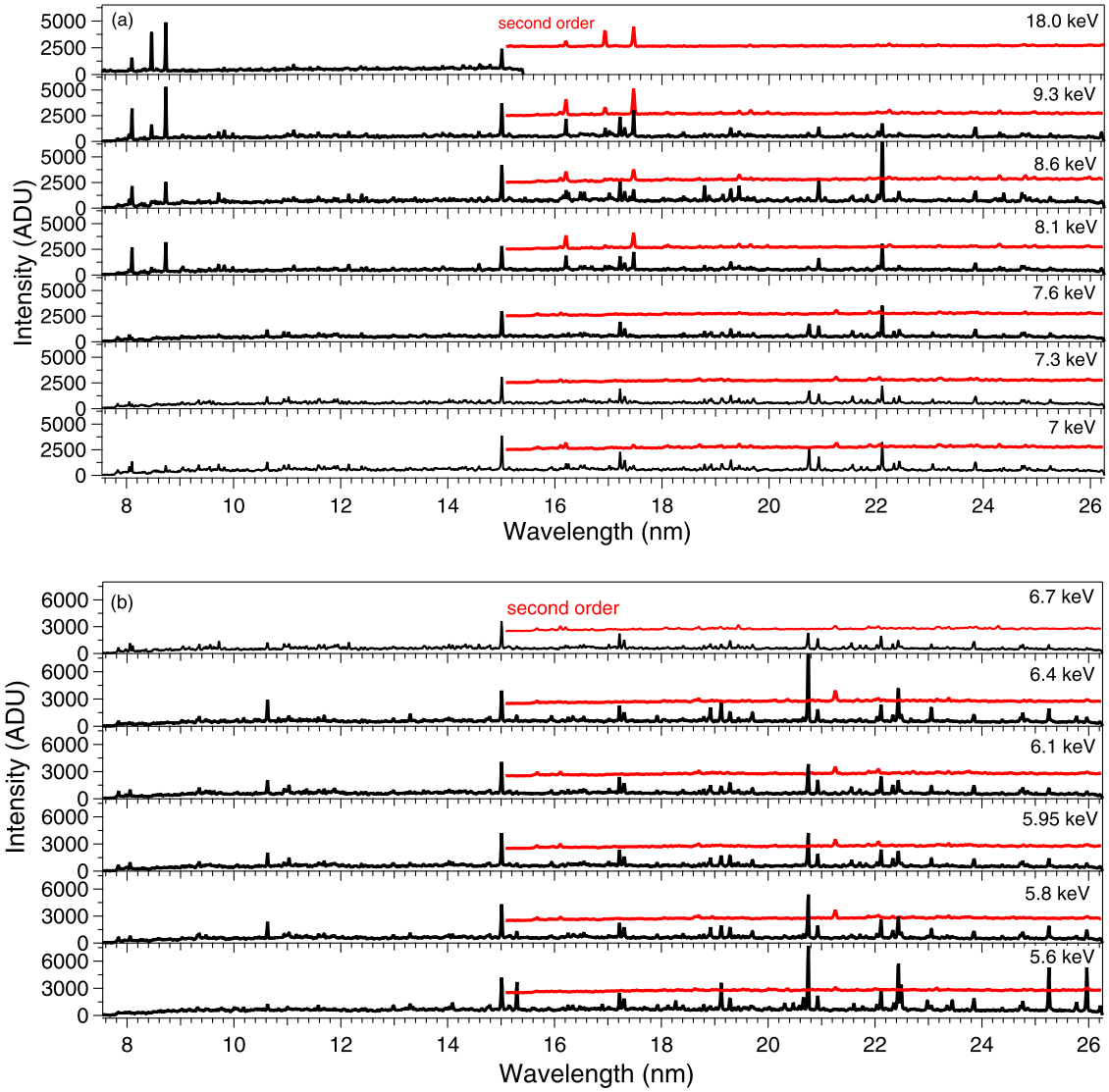


**Figure 1.** Yb spectra that include the Ca-like through Na-like transitions at beam energies between (a) 7 keV and 18 keV and (b) 5.6 keV and 6.7 keV. The vertical shifted lines (red) represent the second-order of diffraction. Note: the indicated nominal beam energy is not space-charge corrected and the intensities are not normalized in time. The detector was moved at the beam energy of 18 keV resulting in an observed wavelength range of 1.8–15.4 nm.

dispersed by a reflection grating with 1200 grooves $mm^{-1}$ and imaged onto a liquid-nitrogen-cooled 2D charge-coupled device (CCD) camera. The EUV spectrum recorded in the CCD pixels was hardware binned to a 1D spectrum. The spectrum in the CCD channels was converted into wavelength in units of nm using well-known lines from highly charged Ne, Ar, and Xe ions [25, 38, 39]. A weighted polynomial function resulted in a calibrated wavelength region of 7.54 nm to 26.25 nm. The weight included the total uncertainty that is a quadrature sum of the adopted wavelength uncertainty from the literature, uncertainty from the line fit, and a constant systematic uncertainty obtained by requiring the reduced chi-square to be 1. The measurement was taken over two days, and the calibrations for the two days were slightly different (but within the overall calibration uncertainties) due to the thermal and electronic fluctuations in the liquid nitrogen cooled detector. The value of the systematic uncertainty was $\pm 0.0006$ nm and $\pm 0.0004$ nm for the two days, respectively, and the residual of the calibration is shown in figure 3.

## 3. Theory

Lines were identified with the aid of simulations performed using the collisional-radiative (CR) non-Maxwellian code NOMAD [40]. Large scale CR modeling requires generation of relevant atomic data such as energies, radiative transition probabilities, autoionization rates, and collisional cross sections from the ground and excited states for electron impact (de-)excitation, ionization, radiative recombination (RR); we have calculated these data using the flexible atomic code (FAC) [41]. The cross sections for inverse processes were obtained using detailed balance principle. We have included the singly-excited configurations up to $n = 6$ or 8 depending upon the complexity of the ion involved and doubly-excited configurations within $n = 3$ shell for all the considered ions. The atomic

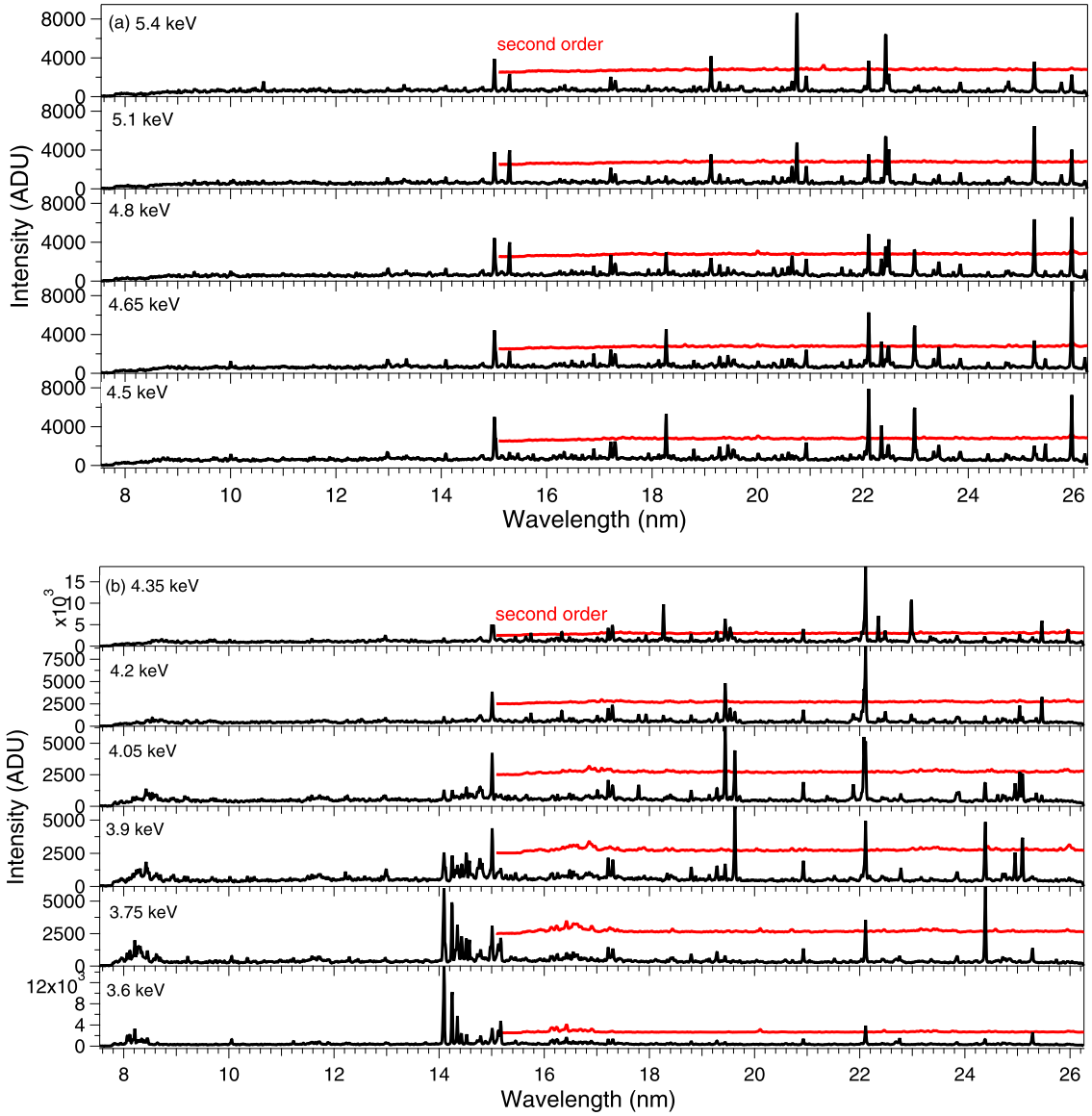


**Figure 2.** Yb spectra that include the Ca-like through Co-like transitions at the beam energies between (a) 4.5 keV and 5.4 keV and (b) 3.6 keV and 4.35 keV. The vertical shifted lines (red) represent the second-order of diffraction. Note: the indicated nominal beam energy is not space-charge corrected and the intensities are not normalized in time.

structure calculations were carried out in the mixed mode which includes $n \leqslant 4$ configurations in the fine-structure and higher configurations ($n > 4$) in the unresolved transition array (UTA) (or relativistic configurations) mode. The calculations in the mixed mode reduce the atomic data and the rate matrix size significantly with negligible changes in the intensities. For example, the number of levels for the Fe-like $Yb^{44+}$ ion (ground state $3d^8$) with singly-excited configurations up to $n = 8$ and double excitations within the M-shell in the mixed mode and fine-structure mode are 2803 and 20 185, respectively. To improve the calculated wavelengths, additional atomic structure calculations were performed by considering all possible excitations within the M-shell as described in previous papers [14, 22, 42]. Thereafter, the original energies of the lower levels in the model were updated with the corresponding energies from the more extensive calculation.

A total of nearly 54 000 levels of 19 ions, from Na-like $Yb^{59+}$ through Cu-like $Yb^{41+}$, were included in the model. Each simulation included 6 or 7 ions depending upon the beam energy and the ionization potential of Yb ions. The ionization balance for the low electron density EBIT plasma is determined by the ionization and recombination between the neighboring charge states, i.e.,

$$\frac{N_{Z+1}}{N_Z} = \frac{n_e\langle\sigma^{ion}_{Z,Z+1}v_e\rangle}{n_e\langle\sigma^{RR}_{Z+1,Z}v_e\rangle + n_e\langle\sigma^{DR}_{Z+1,Z}v_e\rangle + n_o \cdot v_R \cdot \sigma^{CX}_{Z+1,Z}}, \quad (1)$$

where $N_Z$ represent the ion population and $\langle\sigma^{ion}_{Z,Z+1}v_e\rangle$, $\langle\sigma^{RR}_{Z+1,Z}v_e\rangle$, $\langle\sigma^{DR}_{Z+1,Z}v_e\rangle$ are the rate coefficients for ionization (ion), RR, and dielectronic recombination (DR), summed over all channels. $\sigma^{CX}_{Z+1,Z}$ represent the cross sections of charge-exchange (CX) that are directed into the ground state of $Yb^{Z+}$ ions, and $n_o$ and $v_R$ are the density of neutrals and relative

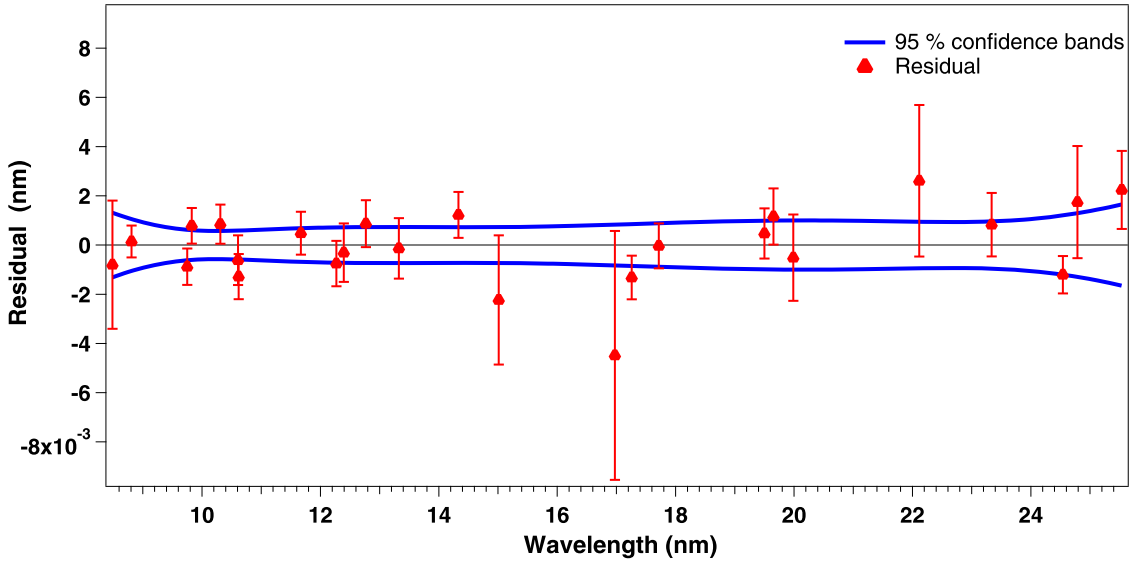


**Figure 3.** Residuals of the calibration data with the total uncertainty given by the error bars as a function of the calibrated wavelength (red data points) along with the 95% confidence bands (blue lines), meaning 95% of the residual should lie within two standard deviation ($\sigma$) of their mean ($\mu$): $P(\mu - 2\sigma \leqslant x \leqslant \mu + 2\sigma) = 0.9545$.

velocity of the ions and neutrals in the trap. $n_e$ and $v_e$ are the electron density and velocity, respectively. DR, being a resonance process, has a negligible effect on the ionization balance in the present EBIT conditions. Radiative and charge exchange recombination are significant for the correct description of the ionization balance.

The charge exchange cross sections, obtained from the classical trajectory Monte Carlo theory, which scale with the ion charge, $Z$, approximately as $Z \times 10^{-15}$ cm$^2$ [43], were used in equation (1) and the rates were included through a free parameter ($n_o \cdot v_R$) in the model. The value of $n_e$ is $10^{11}$ cm$^{-3}$ in our simulations. The ionization balance is independent of electron densities in the absence of CX for the typical values of electron densities for the EBIT plasma which are about $10^{10}$–$10^{12}$ cm$^{-3}$. However, with CX, the ionization balance can change with variation in electron densities which depends upon experimental conditions such as beam current, beam cross sectional area, etc. As mentioned earlier, the free parameter in the model is adjusted to obtain the correct ionization balance to match the observed spectra which also removes the dependency on $n_e$. The value of the free parameter is found to be about $10^{12}$ cm$^{-2}$ s$^{-1}$ to $4 \times 10^{13}$ cm$^{-2}$ s$^{-1}$. The line intensities within the same charge have very weak dependence on the beam energy, and the space charge correction to the beam energy was estimated to be less than 300 eV [35, 37].

The spectra were modeled using a beam energy distribution with a Gaussian profile having full width half maximum of 40 eV, which accurately represents the experimental conditions [44]. The level population, ionization balance, and line intensities were obtained for beam energies in the range of 3.4 keV to 18.0 keV. To account for the instrumental effects associated with the spectrometer, the resultant spectra were convolved with a Gaussian function and corrected for the efficiency curve of the spectrometer [36].

## 4. Results and discussion

The measured spectra were compared to the theoretical spectra for the unambiguous identification of the strong lines. To do so, the theoretical spectra were space charge corrected for proper comparison with the measured spectra. The weaker lines identified in the study were further evaluated by plotting the line intensity of the transitions as a function of the beam energy to determine the charge state based on the ionization energy. Line identification was also assisted by the second- and third-order transitions that arise in the spectra due to the reflection grating in the spectrometer. It has to be noted that a single spectrum contains a mixture of multiply charged ions based on their ionization potential. Furthermore, the transitions from the same charge states can be observed at different beam energies. The final wavelength was therefore determined by computing the weighted average of the wavelength values obtained at different beam energies and different wavelength orders. The wavelength of the transitions observed in second- and third-orders were divided by 2 and 3, respectively, before combining to the first-order values. Comparison of the measured spectra at 6.1 keV with the theoretical spectra at 5.95 keV is shown in figure 4. The dotted lines in the experimental (top) spectra represent the spectral features corresponding to the Ca-like through P-like charge states. These features align with the line features plotted in solid (red) in the theoretical (bottom) spectra. The most abundant charge stage is found to be the K-like Yb ion at this nominal beam energy. Impurity lines from highly charged O, Ar, and N ions are also present in the measured spectra and are indicated with $*$, $+$, and $\circ$, respectively.

For the beam energies of 6 keV and higher, the charge exchange rate in the simulations was increased through the free parameter as described in the previous section in order to obtain better agreement with the measured spectra as shown in

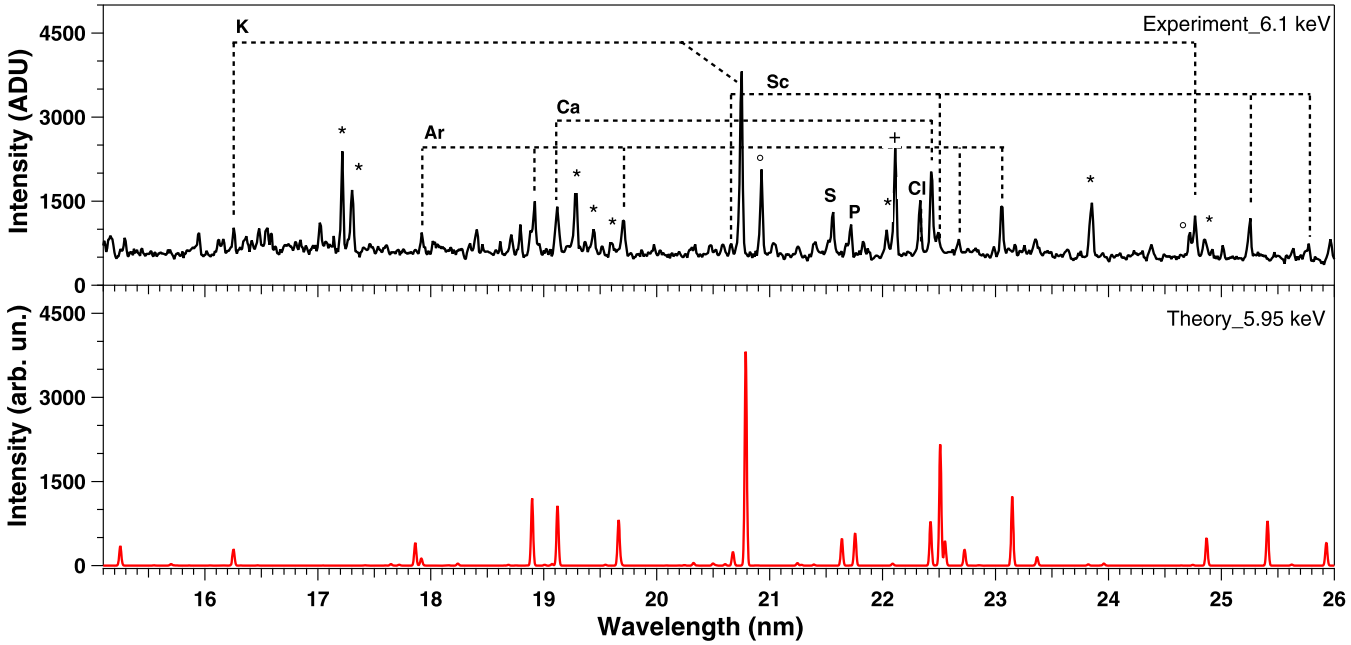


**Figure 4.** Comparison of the experimental spectra at 6.1 keV (top, black) with the theoretical spectra (space-charge corrected) at 5.95 keV (bottom, red). The ∗, +, and ○ symbols correspond to the impurity lines from highly charged O, Ar, and N ions, respectively. The dotted lines correspond to the different ionization stages of Yb.

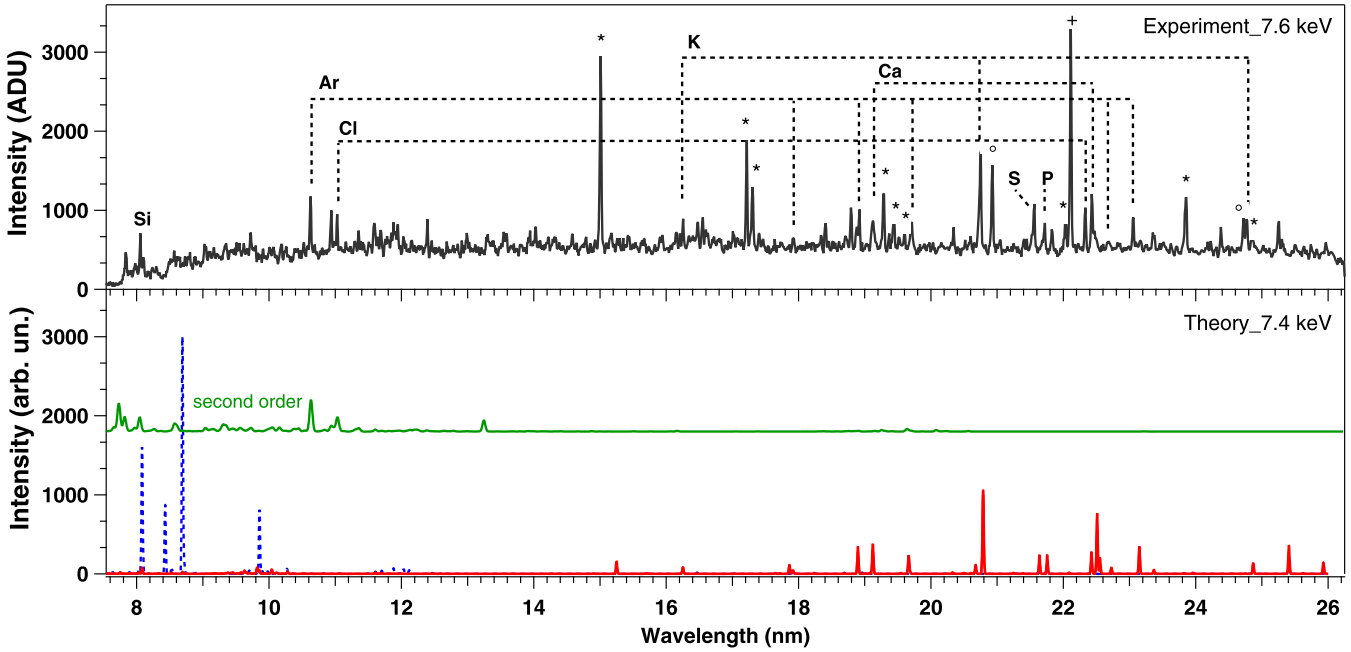


**Figure 5.** Comparison of the measured spectra at 7.6 keV (top, black) with the theoretical spectra (bottom) at 7.4 keV created with a low charge exchange parameter of $8 \times 10^{12}$ cm$^{-2}$ s$^{-1}$ (blue, dotted) and high charge exchange rate (red, solid). The second order of the theoretical spectra with high charge exchange parameter of $3 \times 10^{13}$ cm$^{-2}$ s$^{-1}$ is also shown (offset, green). The ∗, +, and ○ symbols correspond to the impurity lines from highly charged O, Ar, and N ions, respectively. The dotted lines correspond to the different ionization stages of Yb.

figure 5. The free parameter with a value of $8 \times 10^{12}$ cm$^{-2}$ s$^{-1}$ and $3 \times 10^{13}$ cm$^{-2}$ s$^{-1}$ were chosen for the beam energies below and above 6 keV respectively. At beam energies greater than 7 keV, the second-order features of a few highly charged Yb transitions were observed. These transitions are labeled as 'so' in table 1.

We were able to identify 77 lines from the spectra shown in figures 1 and 2, of which 14 are E1 transitions and 63 are M1 transitions. Two sets of UTAs were observed for beam energies in between 3.6 keV and 3.9 keV, first near 8 nm due to the 4p–4d transitions and second near 14 nm from the 4s–4p transitions, corresponding to the Co-like, Mn-like and

**Table 1.** Wavelengths (in nm) of spectral lines of highly charged ions of Yb. The numbers in square brackets are the numbers of lower and upper levels included in the FAC calculations. The numbers in parenthesis are the wavelength uncertainties in the unit of last significant digit[n].

| Ion | Type | Lower level | | Upper level | | $\lambda_{\text{Present}}$ (nm) | | $\lambda_{\text{Previous}}$ (nm) | |
|---|---|---|---|---|---|---|---|---|---|
| | | Conf. | State | Conf. | State | Exp. | FAC | Exp. | Theory |
| 43 [Co] | E1 | $3d^8 4s$ [6] | $((3d^4)_4 4s)_{9/2}$ | $3d^8 4p$ [20] | $((3d^4)_4 4\overline{p})_{9/2}$ | 14.0932(4) | 14.0663 | | |
| 43 [Co] | E1 | $3d^8 4s$ [17] | $((3\overline{d}^3 3d^5)_4 4s)_{7/2}$ | $3d^8 4p$ [32] | $((3\overline{d}^3 3d^5)_4 4\overline{p})_{9/2}$ | 14.5181(5)[bl] | 14.4816 | | |
| 43 [Co] | E1 | $3d^8 4s$ [9] | $((3d^4)_2 4s)_{3/2}$ | $3d^8 4p$ [22] | $((3d^4)_2 4\overline{p})_{5/2}$ | 14.5181(5)[bl] | 14.4986 | | |
| 43 [Co] | E1 | $3d^8 4s$ [7 ] | $((3d^4)_4 4s)_{7/2}$ | $3d^8 4p$ [20] | $((3d^4)_4 4\overline{p})_{9/2}$ | 14.5754(5) | 14.5564 | | |
| 43 [Co] | M1 | $3d^9$ [1] | $(3d^5)_{5/2}$ | $3d^9$ [2] | $(3\overline{d}^3)_{3/2}$ | 24.3855(5) | 24.5994 | 24.355(34)[a] | 24.3879[b]<br>24.3877[b]<br>24.3867[b]<br>24.4026[c] |
| 44 [Fe] | E1 | $3d^7 4s$ [52] | $((3\overline{d}^3(3d^4)_4)_{11/2} 4s)_5$ | $3d^7 4p$ [86] | $((3\overline{d}^3(3d^4)_4)_{11/2} 4\overline{p})_6$ | 14.7765(7)[bl] | 14.7487 | | |
| 44 [Fe] | E1 | $3d^7 4s$ [34] | $((3d^3)_{9/2} 4s)_4$ | $3d^7 4p$ [58] | $((3d^3)_{9/2} 4\overline{p})_5$ | 14.8173(6) | 14.8058 | | |
| 44 [Fe] | M1 | $3d^8$ [1] | $(3d^4)_4$ | $3d^8$ [7] | $(3\overline{d}^3 3d^5)_4$ | 19.6241(6) | 19.6349 | | 19.6552[d]<br>19.4477[e] |
| 44 [Fe] | M1 | $3d^8$ [2] | $(3d^4)_2$ | $3d^8$ [6] | $(3\overline{d}^3 3d^5)_1$ | 22.7820(12) | 22.8810 | | 22.8410[d]<br>22.9148[e] |
| 44 [Fe] | M1 | $3d^8$ [2] | $(3d^4)_2$ | $3d^8$ [5] | $(3\overline{d}^3 3d^5)_2$ | 24.9527(9) | 25.1582 | | 24.9576[d]<br>24.7831[e] |
| 44 [Fe] | M1 | $3d^8$ [1] | $(3d^4)_4$ | $3d^8$ [4] | $(3\overline{d}^3 3d^5)_3$ | 25.0928(6) | 25.3039 | | 25.0771[d]<br>25.1193[e] |
| 45 [Mn] | M1 | $3d^7$ [1] | $(3d^3)_{9/2}$ | $3d^7$ [10] | $(3\overline{d}^3(3d^4)_2)_{7/2}$ | 17.7942(5) | 17.7733 | | |
| 45 [Mn] | M1 | $3d^7$ [1] | $(3d^3)_{9/2}$ | $3d^7$ [9] | $(3\overline{d}^3(3d^4)_4)_{11/2}$ | 19.4408(4) | 19.4499 | | |
| 45 [Mn] | M1 | $3d^7$ [3] | $(3d^3)_{5/2}$ | $3d^7$ [11] | $(3\overline{d}^3(3d^4)_2)_{5/2}$ | 21.8770(7) | 21.8765 | | |
| 45 [Mn] | M1 | $3d^7$ [1] | $(3d^3)_{9/2}$ | $3d^7$ [5] | $(3\overline{d}^3(3d^4)_4)_{9/2}$ | 22.1110(3)[bl] | 22.1528 | | |
| 45 [Mn] | M1 | $3d^7$ [3] | $(3d^3)_{5/2}$ | $3d^7$ [10] | $(3\overline{d}^3(3d^4)_2)_{7/2}$ | 23.8895(8) | 23.9978 | | |
| 45 [Mn] | M1 | $3d^7$ [2] | $(3d^3)_{3/2}$ | $3d^7$ [8] | $(3\overline{d}^3(3d^4)_2)_{1/2}$ | 24.6241(8) | 24.7848 | | |
| 45 [Mn] | M1 | $3d^7$ [1] | $(3d^3)_{9/2}$ | $3d^7$ [4] | $(3\overline{d}^3(3d^4)_4)_{7/2}$ | 25.0401(6) | 25.2269 | | |
| 45 [Mn] | M1 | $3d^7$ [2] | $(3d^3)_{3/2}$ | $3d^7$ [7] | $(3\overline{d}^3(3d^4)_4)_{5/2}$ | 25.3577(13) | 25.5509 | | |
| 46 [Cr] | M1 | $3d^6$ [1] | $(3d^2)_4$ | $3d^6$ [15] | $(3\overline{d}^3(3d^3)_{5/2})_3$ | 15.7449(8) | 15.6704 | | |
| 46 [Cr] | M1 | $3d^6$ [1] | $(3d^2)_4$ | $3d^6$ [12] | $(3\overline{d}^3(3d^3)_{5/2})_4$ | 16.3326(7) | 16.2866 | | |
| 46 [Cr] | M1 | $3d^6$ [2] | $(3d^2)_2$ | $3d^6$ [15] | $(3\overline{d}^3(3d^3)_{5/2})_3$ | 17.2952(7) | 17.2333 | | |
| 46 [Cr] | M1 | $3d^6$ [1] | $(3d^2)_4$ | $3d^6$ [10] | $(3\overline{d}^3(3d^3)_{3/2})_3$ | 19.5327(9)[bl] | 19.5272 | | |
| 46 [Cr] | M1 | $3d^6$ [1] | $(3d^2)_4$ | $3d^6$ [8] | $(3\overline{d}^3(3d^3)_{9/2})_5$ | 22.1110(3)[bl] | 22.1565 | | |
| 46 [Cr] | M1 | $3d^6$ [2] | $(3d^2)_2$ | $3d^6$ [9] | $(3\overline{d}^3(3d^3)_{3/2})_2$ | 22.4831(5) | 22.5446 | | |
| 46 [Cr] | M1 | $3d^6$ [1] | $(3d^2)_4$ | $3d^6$ [5] | $(3\overline{d}^3(3d^3)_{9/2})_4$ | 25.4628(8) | 25.6058 | | |
| 47 [V] | M1 | $3d^5$ [9] | $(3\overline{d}^3(3d^2)_2)_{7/2}$ | $3d^5$ [25] | $((3\overline{d}^2)_0(3d^3)_{9/2})_{9/2}$ | 18.1989(31)[w] | 18.1722 | | |
| 47 [V] | M1 | $3d^5$ [1] | $(3d)_{5/2}$ | $3d^5$ [9] | $(3\overline{d}^3(3d^2)_2)_{7/2}$ | 18.2667(3) | 18.2314 | | |
| 47 [V] | M1 | $3d^5$ [6] | $(3\overline{d}^3(3d^2)_4)_{9/2}$ | $3d^5$ [23] | $((3\overline{d}^2)_2(3d^3)_{5/2})_{7/2}$ | 18.3357(15) | 18.3086 | | |
| 47 [V] | M1 | $3d^5$ [1] | $(3d)_{5/2}$ | $3d^5$ [7] | $(3\overline{d}^3(3d^2)_2)_{5/2}$ | 19.5604(16) | 19.5530 | | |
| 47 [V] | M1 | $3d^5$ [2] | $(3\overline{d}^3(3d^2)_4)_{5/2}$ | $3d^5$ [12] | $((3\overline{d}^2)_2(3d^3)_{9/2})_{7/2}$ | 20.3351(10) | 20.3349 | | |
| 47 [V] | M1 | $3d^5$ [5] | $(3\overline{d}^3(3d^2)_2)_{3/2}$ | $3d^5$ [18] | $((3\overline{d}^2)_2(3d^3)_{3/2})_{5/2}$ | 21.6061(11) | 21.7050 | | |
| 47 [V] | M1 | $3d^5$ [1] | $(3d)_{5/2}$ | $3d^5$ [4] | $(3\overline{d}^3(3d^2)_4)_{11/2}$ | 22.3523(7) | 22.4547 | | |
| 47 [V] | M1 | $3d^5$ [1] | $(3d)_{5/2}$ | $3d^5$ [3] | $(3\overline{d}^3(3d^2)_4)_{7/2}$ | 22.9791(3) | 23.0401 | | |
| 47 [V] | M1 | $3d^5$ [2] | $(3\overline{d}^3(3d^2)_4)_{5/2}$ | $3d^5$ [11] | $((3\overline{d}^2)_2(3d^3)_{9/2})_{5/2}$ | 23.3441(5) | 23.4023 | | |
| 48 [Ti] | M1 | $3d^4$ [4] | $(3\overline{d}^3 3d)_2$ | $3d^4$ [18] | $((3\overline{d}^2)_0(3d^2)_2)_2$ | 14.0857(6) | 14.0050 | | |
| 48 [Ti] | M1 | $3d^4$ [5] | $(3\overline{d}^3 3d)_3$ | $3d^4$ [17] | $((3\overline{d}^2)_0(3d^2)_4)_4$ | 16.8929(4) | 16.8466 | | |
| 48 [Ti] | M1 | $3d^4$ [5] | $(3\overline{d}^3 3d)_3$ | $3d^4$ [16] | $((3\overline{d}^2)_2(3d^2)_0)_2$ | 18.1246(8) | 18.0922 | | |
| 48 [Ti] | M1 | $3d^4$ [1] | $(3\overline{d}^4)_0$ | $3d^4$ [4] | $(3\overline{d}^3 3d)_2$ | 20.3061(9) | 20.2786 | | 20.3438[f] |
| 48 [Ti] | M1 | $3d^4$ [3] | $(3\overline{d}^3 3d)_4$ | $3d^4$ [13] | $((3\overline{d}^2)_2(3d^2)_2)_3$ | 20.4658(5) | 20.4706 | | |

(*continued on next page*)

**Table 1.** Continued

| Ion | Type | Lower level | | Upper level | | $\lambda_{\text{Present}}$ (nm) | | $\lambda_{\text{Previous}}$ (nm) | |
|---|---|---|---|---|---|---|---|---|---|
| | | Conf. | State | Conf. | State | Exp. | FAC | Exp. | Theory |
| 48 [Ti] | M1 | $3d^4$ [4] | $(3\overline{d}^3 3d)_2$ | $3d^4$ [15] | $((3\overline{d}^2)_2(3d^2)_4)_2$ | 20.5836(4) | 20.5863 | | |
| 48 [Ti] | M1 | $3d^4$ [2] | $(3\overline{d}^3 d)_1$ | $3d^4$ [7] | $((3\overline{d}^2)_2(3d^2)_4)_2$ | 21.7667(7) | 21.7892 | | |
| 48 [Ti] | M1 | $3d^4$ [2] | $(3\overline{d}^3 3d)_1$ | $3d^4$ [6] | $((3\overline{d}^2)_2(3d^2)_2)_0$ | 22.1896(7) | 22.2529 | | |
| 48 [Ti] | M1 | $3d^4$ [5] | $(3\overline{d}^3 3d)_3$ | $3d^4$ [13] | $((3\overline{d}^2)_2(3d^2)_2)_3$ | 22.4307(7) | 22.5193 | | |
| 48 [Ti] | M1 | $3d^4$ [4] | $(3\overline{d}^3 3d)_2$ | $3d^4$ [12] | $((3\overline{d}^2)_2(3d^2)_2)_1$ | 22.5725(22) | 22.6214 | | |
| 48 [Ti] | M1 | $3d^4$ [3] | $(3\overline{d}^3 3d)_4$ | $3d^4$ [10] | $((3\overline{d}^2)_2(3d^2)_4)_5$ | 23.4407(5) | 23.5323 | | |
| 49 [Sc] | M1 | $3d^3$ [5] | $((3\overline{d}^2)_2 3d)_{9/2}$ | $3d^3$ [12] | $(3\overline{d}(3d^2)_4)_{11/2}$ | 20.3061(9) | 20.3266 | | |
| 49 [Sc] | M1 | $3d^3$ [1] | $(3\overline{d}^3)_{3/2}$ | $3d^3$ [6] | $((3\overline{d}^2)_2 3d)_{1/2}$ | 20.6560(5) | 20.6753 | | |
| 49 [Sc] | M1 | $3d^3$ [2] | $((3\overline{d}^2)_2 3d)_{5/2}$ | $3d^3$ [8] | $(3\overline{d}(3d^2)_4)_{7/2}$ | 21.6021(9) | 21.6423 | | |
| 49 [Sc] | M1 | $3d^3$ [1] | $(3\overline{d}^3)_{3/2}$ | $3d^4$ [3] | $((3\overline{d}^2)_2 3d)_{3/2}$ | 22.4900(9) | 22.5526 | | |
| 49 [Sc] | M1 | $3d^3$ [4] | $((3\overline{d}^2)_2 3d)_{7/2}$ | $3d^3$ [9] | $(3\overline{d}(3d^2)_4)_{9/2}$ | 23.7163(8) | 23.8214 | | |
| 49 [Sc] | M1 | $3d^3$ [5] | $((3\overline{d}^2)_2 3d)_{9/2}$ | $3d^3$ [9] | $(3\overline{d}(3d^2)_4)_{9/2}$ | 23.8465(8) | 23.9598 | | |
| 49 [Sc] | M1 | $3d^3$ [1] | $(3\overline{d}^3)_{3/2}$ | $3d^3$ [2] | $((3\overline{d}^2)_2 3d)_{5/2}$ | 25.2536(6) | 25.4081 | | |
| 49 [Sc] | M1 | $3d^3$ [4] | $((3\overline{d}^2)_2 3d)_{7/2}$ | $3d^3$ [8] | $(3\overline{d}(3d^2)_4)_{7/2}$ | 25.7685(24) | 25.9238 | | |
| 50 [Ca] | M1 | $3d^2$ [1] | $(3\overline{d}^2)_2$ | $3d^2$ [6] | $(3\overline{d}3d)_1$ | 17.9343(5) | 17.9174 | | |
| 50 [Ca] | M1 | $3d^2$ [1] | $(3\overline{d}^2)_2$ | $3d^2$ [4] | $(3\overline{d}3d)_2$ | 19.1196(6) | 19.1221 | | |
| 50 [Ca] | M1 | $3d^2$ [1] | $(3\overline{d}^2)_2$ | $3d^2$ [3] | $(3\overline{d}3d)_3$ | 22.4334(3) | 22.5109 | | |
| 50 [Ca] | M1 | $3d^2$ [2] | $(3\overline{d}^2)_0$ | $3d^2$ [6] | $(3\overline{d}3d)_1$ | 25.7736(11)[bl] | 25.9237 | | |
| 51 [K] | M1 | $3p^5 3d^2$ [6] | $(3p^3(3\overline{d}^2)_2)_{7/2}$ | $3p^5 3d^2$ [19] | $((3p^3 3\overline{d})_2 3d)_{9/2}$ | 16.2543(5) | 16.2531 | | |
| 51 [K] | M1 | 3d [1] | $(3\overline{d})_{3/2}$ | 3d [2] | $(3d)_{5/2}$ | 20.7485(5) | 20.7884 | | 20.745[g] |
| 51 [K] | M1 | $3p^5 3d^2$ [6] | $(3p^3(3\overline{d}^2)_2)_{7/2}$ | $3p^5 3d^2$ [9] | $((3p^3 3\overline{d})_3 3d)_{9/2}$ | 24.7664(5) | 24.8691 | | |
| 52 [Ar] | E1 | $3p^6$ [1] | $(3p^4)_0$ | $3p^5 3d$ [3] | $(3p^3 3\overline{d})_1$ | 5.3135(4)[so] | 5.3169 | | |
| 52 [Ar] | M1 | $3p^5 3d$ [4] | $(3p^3 3\overline{d})_3$ | $3p^5 3d$ [8] | $(3p^3 3d)_3$ | 17.9208(10) | 17.8624 | | |
| 52 [Ar] | M1 | $3p^5 3d$ [5] | $(3p^3 3\overline{d})_2$ | $3p^5 3d$ [8] | $(3p^3 3d)_3$ | 18.9192(5) | 18.8971 | | |
| 52 [Ar] | M1 | $3p^5 3d$ [3] | $(3p^3 3\overline{d})_1$ | $3p^5 3d$ [7] | $(3p^3 3d)_2$ | 19.7064(5) | 19.6628 | | |
| 52 [Ar] | M1 | $3p^5 3d$ [5] | $(3p^3 3\overline{d})_2$ | $3p^5 3d$ [7] | $(3p^3 3d)_2$ | 22.6723(25) | 22.7260 | | |
| 52 [Ar] | M1 | $3p^5 3d$ [4] | $(3p^3 3\overline{d})_3$ | $3p^5 3d$ [6] | $(3p^3 3d)_4$ | 23.0556(5) | 23.1482 | | |
| 53 [Cl] | E1 | $3p^5$ [1] | $(3p^3)_{3/2}$ | $3p^4 3d$ [3] | $((3p^2)_2 3\overline{d})_{5/2}$ | 5.5141(4)[so] | 5.5171 | | |
| 53 [Cl] | M1 | $3p^4 3d$ [5] | $((3p^2)_2 3\overline{d})_{7/2}$ | $3p^4 3d$ [9] | $((3p^2)_2 3d)_{9/2}$ | 22.3318(4) | 22.4250 | | |
| 53 [Cl] | M1 | $3p^4 3d$ [3] | $((3p^2)_2 3\overline{d})_{5/2}$ | $3p^4 3d$ [8] | $((3p^2)_2 3d)_{7/2}$ | 21.7279(7)[bl] | 21.75697 | | |
| 54 [S] | M1 | $3p^3 3d$ [6] | $(3p3\overline{d})_3$ | $3p^3 3d$ [9] | $(3p3d)_4$ | 21.5696(5) | 21.6392 | | |
| 55 [P] | E1 | $3p^2 3d$ [2] | $(3\overline{d})_{3/2}$ | $3p^3$ [4] | $(3\overline{p}(3p^2)_2)_{5/2}$ | 21.7279(7)[bl] | 21.7553 | | |
| 56 [Si] | E1 | $3p^2$ [2] | $(3\overline{p}3p)_1$ | $3s3p^3$ [4] | $(3s3p)_2$ | 8.0504(11) | 8.0362 | | |
| 57 [Al] | E1 | 3p [1] | $(3\overline{p})_{1/2}$ | $3s3p^2$ [2] | $(3s)_{1/2}$ | 8.1028(4) | 8.0816 | | |
| 57 [Al] | E1 | $3s3p^2$ [2] | $(3s)_{1/2}$ | 3p [3] | $(3p)_{3/2}$ | 9.7218(8) | 9.8559 | | |

(*continued on next page*)

Fe-like Yb ions as seen in figure 2(b). For the beam energies higher than 4.2 keV, these transitions are not observed. For the beam energies between 8.1 keV and 18 keV, the transitions 3s–3p and 3p–3p appear in the wavelength region between 8 nm and 10 nm from M-shell Si-like, Al-like, Mg-like, and Na-like Yb ions. Details of these transitions for different charge states are explained in the sub-sections below. The Co-like through Na-like transitions are shown in figures 1 and 2 respectively.

The wavelength of the identified transitions and the details of the energy levels corresponding to the transitions are listed in table 1. The total uncertainty for the wavelength values is given by the quadrature sum of the line uncertainty from the fit, the systematic uncertainty, and the calibration uncertainty.

**Table 1.** Continued

| Ion | Type | Lower level | | Upper level | | $\lambda_{\text{Present}}$ (nm) | | $\lambda_{\text{Previous}}$ (nm) | |
|---|---|---|---|---|---|---|---|---|---|
| | | Conf. | State | Conf. | State | Exp. | FAC | Exp. | Theory |
| 58 [Mg] | E1 | $3s^2$ [1] | $(3s^2)_0$ | 3s3p [3] | $(3s3\overline{p})_1$ | 8.7351(3) | 8.6919 | | 8.7310[h]<br>8.7389[i]<br>8.7373[j] |
| 59 [Na] | E1 | 3s [1] | $(3s)_{1/2}$ | 3p [2] | $(3\overline{p})_{1/2}$ | 8.4689(5) | 8.4312 | | 8.467[k]<br>8.465[k]<br>8.4693(10)[l]<br>8.470 02[m] |

[a]Reference [19].
[b]Reference [29].
[c]Reference [28].
[d]Reference [49].
[e]Reference [51].
[f]Reference [56].
[g]Reference [57].
[h]Reference [58].
[i]Reference [60].
[j]Reference [27].
[k]Reference [62].
[l]Reference [25].
[m]Reference [24].
[n]Note: superscripts bl, w, and so correspond to (a) the lines that are blended with other features, (b) weak spectral lines, and (c) second order line features, respectively.

The energy level configurations are given in standard relativistic notation $nl$ and $n\overline{l}$ with angular momentum of $j = l + 1/2$ and $j = l - 1/2$, respectively. Here, $n$ is the principal quantum number, and $l$ represents the orbital quantum number.

### 4.1. *Co-like* $Yb^{43+}$

We identified four E1 spectral lines corresponding to the $3d^8 4s–3d^8 4p$ transitions, of which some spectral lines are blended with other Co-like features, shown in figure 2(b). These blended transitions have been labeled as 'bl' in table 1. One M1 transition $^2D_{3/2} \rightarrow {}^2D_{5/2}$ within the ground configuration $3d^9$ of Co-like Yb ions was also observed in this measurement. The forbidden transition within the ground configurations having one vacancy in a closed shell offers tests to probe the relativistic and QED effects [28, 29]. These transitions are stronger in highly charged high-$Z$ ions as their rates show a strong dependence on nuclear charge [45]. The $3d^9\ {}^2D_{3/2} \rightarrow {}^2D_{5/2}$ transitions have been observed for Co-like ions of $Zr^{13+}$, $Nb^{14+}$, $Mo^{15+}$, $Hf^{45+}$, $Ta^{46+}$, $W^{47+}$, and $Au^{52+}$ [31, 42, 46]. Our reported value of 24.3855(5) nm for this transition in $Yb^{43+}$ agrees with the predicted value of 24.355(34) nm [19], obtained from the extrapolations of the fitted values of the $^2D_{3/2} \rightarrow {}^2D_{5/2}$ fine-structure interval. Their reported uncertainty is obtained by assuming the calculated values of the fitting function to be uncertain by +0.0005 from $Z = 38$ to 42, by +0.0010 from $Z = 43$ to 64, and by amounts varying from 0.001 to 0.003 from $Z = 64$ to 92. The wavelengths of this forbidden M1 transition in Co-like ions were calculated for elements with $28 \leqslant Z_N \leqslant 100$ using different theoretical approaches such as MCDHF, RMBPT, and MCDHF-FCV (full core valence correlation) [28, 29]. Our result is also in fair agreement with their calculated values of 24.3879 nm, 24.3877 nm, and 24.3867 nm obtained by using MCDHF-FCV, MCDHF, and RMBPT methods [29], respectively.

A recent and more advanced MCHDF calculation [28] of this transition gives 24.4026 nm for the wavelength, which disagrees with our measurement and the calculations previously discussed. Using the GRASP2K code, similar to [29], the authors in [28] included the frequency-dependent Breit interaction as well as several modifications of QED contributions which resulted in comparable values. Nonetheless, the calculated results are well outside of the uncertainties of our previous measured wavelengths for high-$Z$ ions [31, 42]. Our present measured value of 24.3855(5) nm follows the observed experimental trend, and with a factor-of-six smaller uncertainties, it offers a new challenge for modern atomic theories. It is worth noting that Co-like ions with the $3d^9$ ground configuration present an example of 'Layzer quenching' with suppressed correlations and enhanced relativistic and QED effects [47]. Similar to previous work with F-like ions (see, e.g., [48]), new calculations for Co-like ions may be required to explain the measurements.

### 4.2. *Fe-like* $Yb^{44+}$

No measured transitions for the Fe-like $Yb^{44+}$ charge state have been reported in the EUV region so far. In this measurement, we identified two dipole-allowed lines from the $3p^7 4s–3p^7 4p$ transitions in the Fe-like $Yb^{44+}$ ion. We also observed four forbidden M1 features at

wavelengths of 19.6241(6) nm, 22.7820(10) nm, 24.9527(9) nm, and 25.0928(6) nm arising from transitions within the $3d^8$ ground configuration. Ekberg *et al* [49] reported the predicted energy values for the levels within the $3p^6 3d^8$ configuration obtained from parametric fitting of the differences in the calculated level values using Grant code [50] and the observed values. From these predicted values, the calculated M1 transitions were 19.6552 nm, 22.8410 nm, 24.9576 nm, and 25.0771 nm, respectively, for the $(3d^8)_4$–$(3d^8)_4$, $(3d^8)_2$–$(3d^8)_1$, $(3d^8)_2$–$(3d^8)_2$, and $(3d^8)_4$–$(3d^8)_3$ transitions. The large discrepancies of the energy levels from their extrapolated values is reported to the order of 1500 $cm^{-1}$. Our measured wavelengths are also different from the values reported by Ivanova and Tsirekidze [51] obtained with *ab initio* calculations. Their calculated values for these transitions are 19.4477 nm, 22.9148 nm, 24.7831 nm, and 25.1193 nm. They do not report the discrepancy from observed values for $Z_N > 60$ in their study but note that around $Z_N$ of 60, the discrepancy is close to 1000 $cm^{-1}$.

### 4.3. *Mn-like* $Yb^{45+}$–*V-like* $Yb^{47+}$

Eight M1 transitions within the $3d^7$ ground configuration were observed for Mn-like Yb ions. Seven M1 transitions within the ground $3d^6$ configuration were observed for the Cr-like Yb ions. The Cr-like transition at FAC wavelength of 22.1565 nm is blended with a Mn-like transition at FAC wavelength of 22.1528 nm. This line is reported at a measured wavelength of 22.1110(3) nm and labeled as bl in table 1. Nine M1 forbidden transitions within the ground $3d^5$ configuration were identified for the V-like Yb ions. No calculations or observations of these transitions have been reported before.

### 4.4. *Ti-like* $Yb^{48+}$–*K-like* $Yb^{51+}$

Eleven M1 transitions corresponding to Ti-like $Yb^{48+}$ within the $3d^4$ configurations were observed between the wavelength region of 14 nm and 24 nm. Previous experimental [52] and theoretical [53–56] works have studied the forbidden optical M1 transitions in highly charged Ti-like ions near the UV region (300 nm to 400 nm) due to the relevance of these intense lines in plasma diagnostics as well as in complex atomic structure and correlation studies, but the wavelength region considered here is less explored. From the calculated energy levels of the $3d^4$ configuration in Ti-like ions reported by Feldman *et al* [56], the transition wavelength of 20.3438 nm for the $(3d^4)_0$–$(3d^4)_2$ transition agrees very roughly with to our measured value of 20.3061(9) nm. Their work reported the energies of the lowest $J = 1$ through $J = 4$ levels; however, most of our identified Ti-like spectral lines arise from transitions between higher energy levels.

Eight Sc-like M1 transitions within the $3d^3$ configuration were identified in this work. We also identified four Ca-like M1 transitions within the $3d^2$ configurations. No previous calculations or measurements of these forbidden transitions were found.

Three K-like M1 transitions were identified, of which the emissions at 16.2543(5) nm and 24.7664(5) nm were a result of transition between energy levels in the $3p^5 3d^2$ configuration. The strongest line at 20.7485(5) nm in figure 4 is due to the fine-structure splitting between the $3p^6 3d\ D_J$, $J = 3/2$ and $J = 5/2$ levels of K-like ions. This splitting was calculated by Ali and Kim [57] with multi-configuration wave functions to be 20.745 nm. The accuracy of this result is not provided in their report; however, it is close (1% discrepancy at 7 std. dev.) to our measured value.

### 4.5. *Ar-like* $Yb^{52+}$–*Al-like* $Yb^{59+}$

The ground state configuration changes to $3s^2 3p^k$ ($k = 1$–6) for the Al-like $Yb^{57+}$ through Ar-like $Yb^{52+}$ ions. We observed the second-order of the E1 transition $3p^6$–$3p^5 3d$ with wavelength of 5.3135(4) nm for the Ar-like charge state. Five M1 transitions within the $3p^5 3d$ configuration were also identified in the measured spectra from Ar-like Yb ions. Similarly, the second-order of the $3p^5$–$3p^4 3d$ transition with wavelength of 5.5141(4) nm was observed for the Cl-like charge state. Two Cl-like M1 transitions within the $3p^4 3d$ configuration and one S-like M1 transition within $3p^3 3d$ configuration were identified. One E1 line from $3p^2 3d$–$3p^3$ transition was identified for the P-like Yb ion, which is blended with a Cl-like transition at FAC value of 21.75697 nm. A Si-like Yb spectral feature from the $3p^2$–$3s3p^3$ transition was observed at 8.0504(11) nm. Another E1 line close to this wavelength was identified as an Al-like transition at 8.1028(4) nm. We identified one more E1 line from the Al-like charge state due to the $3s3p^2$–$3s^2 3p$ transition at 9.7218(8) nm.

### 4.6. *Mg-like* $Yb^{58+}$

Since the Mg-like systems have two electrons outside the Ne-like core, these systems are relevant in theoretical studies of core–valence and core–core correlations in atomic structure calculations [26]. Such studies have been performed theoretically along the Mg-like isoelectronic sequence [26, 27]. Santana and Träbert performed *ab initio* calculations using the multireference Møller–Plesset many-body perturbation theory for $Z_N = 15$–92 [58]. Their study improved the agreement with experiment to within 100 ppm over a wide range of $Z_N$. However, the authors stress that there is less experimental data available for $Z_N > 55$, including data with larger error bars for $Z_N > 55$ [59]; thus, more accurate measurements are necessary to constrain calculations in the high-$Z_N$ region where relativistic and QED effects are massive. Their calculated value of 8.7310 nm [58], in contrast to the higher value of 8.7389 nm from the MCDHF and relativistic configuration interaction calculations [60] and 8.7373 nm from the MCDHF calculations [27], is much close to but lower than our measured value of 8.7351(3) nm, with a discrepancy of 4.6 parts in $10^4$.

### 4.7. *Na-like* $Yb^{59+}$

Na-like ions behave as quasi-hydrogenic ions with just one electron outside the closed Ne-like core. The Na-like resonance $3s_{1/2}$–$3p_{1/2}$ (D1) and $3s_{1/2}$–$3p_{3/2}$ (D2) transitions are known for their precise *ab initio* calculations as well as accurate measurements. In this work, we measured the $3s_{1/2}$–$3p_{1/2}$ D1 transition at a wavelength value of 8.4699(5) nm. This transition has been calculated in previous studies; however,

this is the first reported measured value of the transition. Studies of the transition wavelengths of the strong Na-like highly charged systems [25] were performed to test the accuracy of QED theory, and these systems are considered sensitive to nuclear size effects [25, 61]. In a study by Kim *et al* [62], qualitative features in the $Z_N$ dependence of relativistic correlation energy and QED corrections of Na-like ions including Li- and Cu-like ions are discussed, and theoretical and interpolated/extrapolated transition wavelengths for the resonance $3s_{1/2}-3p_{1/2}$ transition are determined to be 8.467 nm and 8.465 nm, respectively. Our measured value of 8.4689(5) nm agrees well with the calculated value of 8.4693(10) nm obtained with the RMBPT theory [25] and the calculated value of 8.47002 nm obtained by the *S*-matrix method [24].

## 5. Conclusions

We observed 77 spectral features from Co-like Yb through Na-like Yb ions in the wavelength region between 7.5 nm and 26.2 nm, of which 76 are new. These transitions were dominated by the M1 transitions within the $3d^k$ configurations ($k$ = 1–9) for the Co-like Yb through K-like Yb ions and within the $3p^k3d$ configurations ($k$ = 3–5) for the Ar-like Yb through S-like ions. The wavelengths of these lines were measured with uncertainties between ±0.0003 nm for the strongest lines and ±0.0031 nm for the weakest lines. The FAC and the non-Maxwellian code NOMAD was used to identify the line features. Our identification of previously unobserved transitions in highly charged Yb can be useful to benchmark tests of the existing theoretical framework.

## Acknowledgments

This work was funded by the Measurement Science and Engineering (MSE) Research Grant Programs of the Department of Commerce at NIST, Award No. 70NANB19H024 and 70NANB20H87. J M D acknowledges support from a National Research Council Associateship award at NIST.

## Data availability statement

The data generated and/or analysed during the current study are not publicly available for legal/ethical reasons but are available from the corresponding author on reasonable request.

## ORCID iDs

R Silwal https://orcid.org/0000-0003-4175-4135
Dipti https://orcid.org/0000-0001-6675-8509
E Takacs https://orcid.org/0000-0002-2427-5362
J M Dreiling https://orcid.org/0000-0001-9226-203X
A C Gall https://orcid.org/0000-0002-8260-2229
Yu Ralchenko https://orcid.org/0000-0003-0083-9554

## References

[1] Hinkley N, Sherman J A, Phillips N B, Schioppo M, Lemke N D, Beloy K, Pizzocaro M, Oates C W and Ludlow A D 2013 *Science* **341** 6151
[2] Huntemann N, Okhapkin M, Lipphardt B, Weyers S, Tamm C and Peik E 2012 *Phys. Rev. Lett.* **108** 090801
[3] Schneider T, Peik E and Tamm C 2005 *Phys. Rev. Lett.* **94** 230801
[4] Tamm C, Weyers S, Lipphardt B and Peik E 2009 *Phys. Rev.* A **80** 043403
[5] Safronova M S, Budker D, DeMille D, Jackson Kimball D F, Derevianko A and Clark C W 2018 *Rev. Mod. Phys.* **90** 025008
[6] Biémont E, Quinet P, Dai Z, Zhankui J, Zhiguo Z, Xu H and Svanberg S 2002 *J. Phys. B: At. Mol. Opt. Phys.* **35** 4743
[7] Karaçoban B and Özdemir L 2011 *Z. Nat.* A **66** 543–51
[8] Counts I *et al* 2020 *Phys. Rev. Lett.* **125** 123002
[9] Zeng G M *et al* 1994 *J. Appl. Phys.* **75** 1923
[10] O'Sullivan G and Carroll P K 1981 *J. Opt. Soc. Am.* **71** 227
[11] O'Sullivan G *et al* 2015 *J. Phys. B: At. Mol. Opt. Phys.* **48** 144025
[12] Kilbane D, O'Sullivan G, Gillaspy J D, Ralchenko Y and Reader J 2012 *Phys. Rev.* A **86** 042503
[13] Kilbane D, Gillaspy J D, Ralchenko Y, Reader J and O'Sullivan G 2013 *Phys. Scr.* **T156** 014012
[14] Kilbane D, O'Sullivan G, Podpaly Y A, Gillaspy J D, Reader J and Ralchenko Y 2014 *Eur. Phys. J.* D **68** 222
[15] Suzuki C, Koike F, Murakami I, Tamura N and Sudo S 2018 *Atoms* **6** 24
[16] Blundell S A, Johnson W R, Safronova M S and Safronova U I 2008 *Phys. Rev.* A **77** 032507
[17] Finkenthal M, Moos H W, Bar-Shalom A, Spector N, Zigler A and Yarkoni E 1988 *Phys. Rev.* A **38** 288
[18] Daido H, Ninomiya S, Takagi M and Kato Y 1999 *J. Opt. Soc. Am.* B **16** 2
[19] Ekberg J O, Reader J, Acquista N, Feldman U, Seely J F and Brown C M 1987 *J. Opt. Soc. Am.* B **4** 1913–8
[20] Reader J 1983 *J. Opt. Soc. Am.* **73** 63–5
[21] Suzuki C *et al* 2017 *Plasma Phys. Control. Fusion* **59** 014009
[22] Podpaly Y A, Gillaspy J D, Reader J and Ralchenko Y 2014 *J. Phys. B: At. Mol. Opt. Phys.* **48** 2
[23] Dipti , Silwal R, Dreiling J M, Sanders S C, Takacs E and Ralchenko Y 2020 *J. Phys. B: At. Mol. Opt. Phys.* **53** 145002
[24] Sapirstein J and Cheng K T 2015 *Phys. Rev.* A **91** 062508
[25] Gillaspy J D, Osin D, Ralchenko Y, Reader J and Blundell S A 2013 *Phys. Rev.* A **87** 062503
[26] Iorga C and Stancalie V 2018 *At. Data Nucl. Data Tables* **123–124** 313–28
[27] Zou Y and Fischer C F 2001 *J. Phys. B: At. Mol. Opt. Phys.* **34** 5
[28] Si R, Guo X L, Brage T, Chen C Y, Hutton R and Froese Fischer C 2018 *Phys. Rev.* A **98** 012504
[29] Guo X L *et al* 2016 *Phys. Rev.* A **93** 012513
[30] Edlén B 1984 *Phys. Scr.* **T8** 5–9
[31] Ralchenko Y, Draganić I N, Osin D, Gillaspy J D and Reader J 2011 *Phys. Rev.* A **83** 032517
[32] Yudin V I, Taichenachev A V and Derevianko A 2014 *Phys. Rev. Lett.* **113** 233003
[33] Fahy K, Sokell E, O'Sullivan G, Aguilar A, Pomeroy J M, Tan J N and Gillaspy J D 2007 *Phys. Rev.* A **75** 032520
[34] Holland G E, Boyer C N, Seely J F, Tan J N, Pomeroy J M and Gillaspy J D 2005 *Rev. Sci. Instrum.* **76** 073304
[35] Silwal R, Takacs E, Dreiling J, Gillaspy J and Ralchenko Y 2017 *Atoms* **5** 30
[36] Blagojević B *et al* 2005 *Rev. Sci. Instrum.* **76** 083102

[37] Porto J V, Kink I and Gillaspy J D 2000 *Rev. Sci. Instrum.* **71** 3050
[38] Osin D, Reader J, Gillaspy J D and Ralchenko Y 2012 *J. Phys. B: At. Mol. Opt. Phys.* **45** 245001
[39] Kramida A, Ralchenko Y and Reader J (NIST ASD Team) 2020 *NIST Atomic Spectra Database (Version 5.8)* (Gaithersburg, MD: National Institute of Standards and Technology) https://physics.nist.gov/asd
[40] Ralchenko Y and Maron Y 2001 *J. Quant. Spectrosc. Radiat. Transfer* **71** 609–21
[41] Gu M F 2008 *Can. J. Phys.* **86** 675–89
[42] Osin D, Gillaspy J D, Reader J and Ralchenko Y 2012 *Eur. Phys. J.* D **66** 286
[43] Otranto S, Olson R E and Beiersdorfer P 2006 *Phys. Rev.* A **73** 022723
[44] Gall A C, Dipti , Buechele S W, Sanders S, Szabo C I, Silwal R, Ralchenko Y, Brickhouse N and Takacs E 2020 *J. Phys. B: At. Mol. Opt. Phys.* **53** 145004
[45] Ralchenko Y and Gillaspy J D 2013 *Phys. Rev.* A **88** 012506
[46] Prior M H 1987 *J. Opt. Soc. Am.* B **4** 144
[47] Li M C, Si R, Brage T, Hutton R and Zu Y M 2018 *Phys. Rev.* A **98** 020502
[48] O'Neil G *et al* 2020 *Phys. Rev.* A **102** 032803
[49] Ekberg J O, Reader J and Feldman U 1988 *J. Opt. Soc. Am.* B **5** 1275–84
[50] Grant I P, McKenzie B J, Norrington P H, Mayers D F and Pyper N C 1980 *Comput. Phys. Commun.* **21** 207
[51] Ivanova E P and Tsirekidze M A 1986 *Phys. Scr.* **34** 35
[52] Watanabe H, Crosby D, Currell F J, Fukami T, Kato D, Ohtani S, Silver J D and Yamada C 2001 *Phys. Rev.* A **63** 042513
[53] Fischer C F and Fritzsche S 2001 *J. Phys. B: At. Mol. Opt. Phys.* **34** L767L772
[54] Kato D, Yamada C, Fukami T, Ikuta I, Watanabe H, Okazaki K, Tsurubuchi S and Ohtani S 1999 *Phys. Scr.* **T80** 446–7
[55] Biémont E, Träbert E and Zeippen C J 2001 *J. Phys. B: At. Mol. Opt. Phys.* **34** 1941–51
[56] Feldman U, Indelicato P and Sugar J 1991 *J. Opt. Soc. Am.* B **8** 1
[57] Ali M A and Kim Y-K 1992 *J. Opt. Soc. Am.* B **9** 2
[58] Santana J A and Träbert E 2015 *Phys. Rev.* A **91** 022503
[59] Gillaspy J D, Draganić I N, Ralchenko Y, ReaderJ , Tan J N, Pomeroy J M and Brewer S M 2009 *Phys. Rev.* A **80** 010501
[60] Hu F, Mei M, Han C, Han B, Jiang G and Yang J 2014 *J. Quant. Spectrosc. Radiat. Transfer* **149** 158–67
[61] Silwal R *et al* 2018 *Phys. Rev.* A **98** 052502
[62] Kim Y-K, Baik D H, Indelicato P and Desclaux J P 1991 *Phys. Rev.* A **44** 148–66